Taylor & Francis
Taylor & Francis Group

∂ OPEN ACCESS · Check for updates

Kaolinite under pressure at audio frequency range and its electrical features

Mohamed Mahmoud Gomaa

Geophysical Sciences Dept., National Research Center, Cairo, Egypt

ABSTRACT

Electrical features of a humid kaolinite specimens was measured at various pressures and at various frequencies . Surface impedance is supposed on kaolinite particle surfaces (from humidity), chemical reaction and charge transport along surface hydroxyls of kaolinite edges besides the permanent negative charges. Classic mixture laws do not support the interpretation of electrical properties, especially, at high pressures. Accordingly, interpretation was made with percolation threshold theories. Pressure increase causes decrease in pore spaces and accordingly increases possible connections of pore distances filled with humidity to total pore spaces after applying pressure. With pressure increase, the pore voids between particles decrease and water conducting paths increase. Also, dielectric constant and conductance increase with increase of pressure. On the other hand, at a certain pressure, at low frequencies, a noticeable increase of capacitance with pressure increase, that tends to reach constant value, for relatively high pressures. The diffusion and interfacial mechanisms was suggested to interpret samples with increase of pressure and frequency. The latter mechanism acts simultaneously with surface chemical reaction mechanism (Debye behavior) to give a depressed arc (relaxation time distribution). Finally, the pressure and frequency are effective factors on electrical properties.

1. Introduction

Few studies show the effect of increasing pressure on electrical features of rocks (Hussain 1981, 1997). Kaolinite is a porous medium. Generally, it behaves as a random two-phase system (double electrical layers between particles or pore space and kaolinite particle space) separated by random (and discrete) humid interfaces. Pores in kaolinite particles give a degree of interconnection, via what are called pore throats. They may contain some free water and, if ions are found in it, an electrolyte as well. Adsorbed discrete water is, usually, found at the particle surface due to humidity. Each of these phases contributes to the electrical features (Hussain 1997; Gomaa 2008, 2009).

Schwarz (1962) studied the dielectric dispersion, for relatively low frequencies, of colloidal particles, in liquid solutions that contain ions. Schwarz (1962) suggested the existence of diffusion-controlled polarisation around the particles, which controls the dielectric dispersion at low frequencies. He suggested that an electric field would result in a counteracting diffusion flux with the flux induced by the impressed electric field (Levitskaya 1984; Levitskaya and Sternberg 1996a, 1996b). He derived a relation between relaxation time, the radius of the particle and mobility. Schwarz (1962) suggested that at the surfaces of wet clay particles there exists a tangential diffusion-controlled polarisation around the surface resulting from the counter-ions, which are strongly bound to the surface by electrostatic

attraction (Klein and Sill 1982; Garrouch and Sharma 1994). At moderate mobility of charges, the complex surface conductivity λ_s was described by Debye behaviour (Ruffet et al. 1991), responsible for dispersion at lower radio frequencies:

$$\lambda_S = \frac{iW\tau}{1 + iW\tau}\lambda_0 \qquad (1)$$

w is angular frequency, λ_0 is the DC surface conductivity and τ is the relaxation time constant.

At relatively high frequencies, surface conductivity equals $\lambda_s = \lambda_0$ and,

$$\lambda_0 = e_n^2 s_d u_m \qquad (2)$$

where e_n is the electric charge, s_d is the density of surface charges (ions per unit area), which can move only tangentially or horizontally over the surface, u_m is the mechanical mobility (i.e. velocity per unit force), and τ is the relaxation time;

$$\tau = \frac{R^2}{2u_m KT} \qquad (3)$$

where R is the radius of the particle, T is the temperature and K is the Boltzman constant.

Brace et al. (1965) measured the DC electrical resistivity of eight igneous rocks and two crystalline limestones at pressures up to $10Kb$. The rocks were saturated with drinking water or salt solution. The porosity of some rocks was found to be less than 0.001. Resistivity increases with an increase in

---

CONTACT Mohamed Mahmoud Gomaa ✉ mmmsgomaa@yahoo.com 🖳 Geophysical Sciences Dept., National Research Center, Cairo, Egypt

pressure. Resistivity changes were quick for the first 2 *Kb* and progressively decreased for high pressures. The data suggest two kinds of conduction in these rocks: (1) conduction along cracks (at a pressure of a few kilobars) as in granite (Abou El-Anwar and Gomaa 2013, 2016), and (2) volume and surface conduction along a network of pores that continue over the whole pressure range (remaining open for relatively higher pressure), as in sand. A rock saturated with drinking water has a surface conduction 10 to 20 times greater than conduction mechanisms from pore volumes (Gomaa et al. 2019, Khater et al. 2019a, 2019b; Melegy et al. 2019; Gomaa 2020; Gomaa and Kenawy 2020). Rocks of minute porosity under low pressure may show a transition behaviour from a resistive condition to a conductive condition. But if minute water films persist within interstices in spite of fairly high pressure, the resistivity might be orders of magnitude greater than the frequency under dry conditions up to percolation pressures (high pressures) (Jonscher 1973, 1975, 1977, 1999a, 1999b).

Olhoeft (1977) measured the dielectric constant and resistivity of natural clays specimens with an applied uniaxial load up to 2 *Kb*. The frequency range used was from $10 Hz$ to 10^6 Hz. The resistivity decreased with increasing pressure from 10^6 to $10^5 Hz$ of frequency range. Above $10^5 Hz$ the dependence on pressure disappeared completely. The dielectric constant increases with increasing pressure. Olhoeft noticed a mechanism, similar to that given by Maxwell–Wagner, that has an effect that increases as pressure increases. A model was assumed by Olhoeft (1977) for relaxation time collections with several possible relaxation mechanisms. Each mechanism has a characteristic relaxation time. These mechanisms, when acting simultaneously, may display relaxation time collections (Bockris et al. 1966; Borner et al. 1993).

Hussain (1997) used a model to describe the electrical effects of relative atmospheric humid kaolinite ($10^5 Hz$) based on mechanisms assumed to take place on clay particle interfaces and trace water present in the pore spaces surrounding such particles (Arulanandan 1969). He tried to describe the electrical effect of clay under pressure up to $\approx 4.5 Kb$. He made a representation of the Z-plane under various pressures (Chew and Sen 1982; Shaltout et al. 2012). These data showed a relaxation time collection due to application of various pressures. Resistance decreases, and capacitance increases, with increasing pressure. He suggested that the chemical reaction impedance in clay resulted from charge disconnection and the charge transport process.

The difficulty in interpreting experimental data from clay is expressed by considering interface effects in non-metallic conducting solids and liquids (Macdonald 1980). The following physical processes
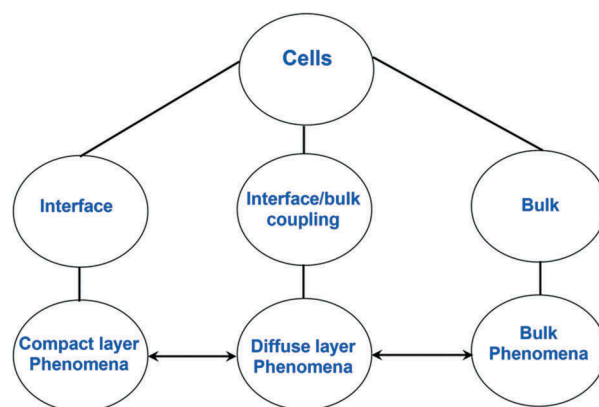

Figure 1. Schematic representation diagram showing some bulk–interphase relations.

are usually included and some or all of them may be important in specific cases: (a) charge transport – conduction and diffusion; (b) generation/recombination of charged species; (c) neutral species transport – diffusion in material and/or electrodes; (d) adsorption/desorption at the electrodes; and (e) charge transfer (redox reactions) at the electrodes.

The first two effects (a and b) occur in material bulk specimens, whereas (d) and (e) are the result of the interface of the particles on the samples, and (c) occurs in either the bulk or at an electrode (or possibly both). A diagram showing the interaction of the processes present in an electrode/material situation is presented in Figure 1.

The intention is to try to interpret experimental data for kaolinite samples under pressures of up to $\approx 4.5 Kb$ ($\approx 50\%$ relative atmospheric humidity), at frequencies 10 Hz to 10 Hz.

2. Methodology

A Hioki 3522–50 LCR Hitester Impedance Analyzer was used to measure electrical characteristics (Gomaa and Elsayed 2006). The geometry of the samples was chosen to reduce errors due to stray capacitance. Specimen edges were polished to make them parallel. Electrical features were measured at frequencies from 10 Hz up to 10^4 Hz, using non-polarising (four) electrodes (Cu/CuSO$_4$) at an applied voltage of 1 volt (Gomaa and Alikaj 2009).

Electrical features were measured (Hioki 3522–50 LCR) using either series or parallel configuration (Figure 2). Parallel capacitance and conductance (10^4 and G_p) and series impedance (Z) at various frequencies were measured (Gomaa and Elsayed 2009). Complex permittivity was calculated from the equation:

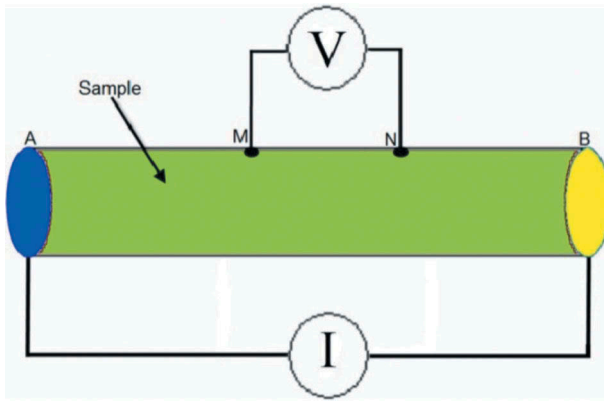$$\varepsilon^* = \varepsilon' - i\varepsilon'' \tag{4}$$

Figure 2. Schematic representation of the sample holder.

$$\varepsilon' = C_p d/\varepsilon_0 A \qquad (5)$$

is real and imaginary permittivity

$$\varepsilon'' = G_p d/\omega\varepsilon_0 A \qquad (6)$$

where A is the cross-sectional area of specimen, d is the specimen thickness, $\varepsilon_0 = 8.85 \times 10^{-12}$(F/m) is the free space permittivity and ω is the angular frequency. The real conductivity is:

$$\sigma' = G_p d/A = \varepsilon'' \omega\varepsilon_0 \qquad (7)$$

Real impedance = R_s, imaginary impedance = $1/w \times C_S$, R_s and C_s are series resistance and capacitance, respectively.

2.1. Material used

Kaolin consists principally of the mineral kaolinite $(Al_2Si_2O_5(OH)_4.4H_2O)$, and contains varying amounts of other minerals such as muscovite, quartz, feldspar and anatase Figure 3. Kaolin occurs as an odourless white to yellowish or greyish powder (Lockhart 1980; Leroy and Revil 2004; Cosenza et al.
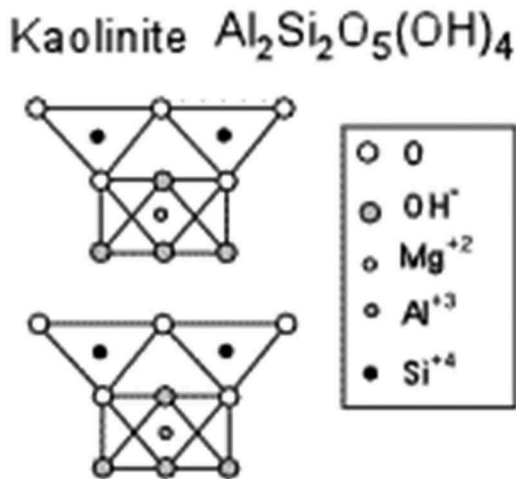

Figure 3. Active surface sites at the edge of the kaolinite.

2008; Jougnot et al. 2009; Leroy and Revil 2009). Kaolin is insoluble in water but darkens and develops an earthy odour when wet. It can be distinguished from other industrial clays based on its fine particle size and pure colouring. Its ability to disperse in water makes it an ideal pigment. The white colour of the mineral can be naturally occurring, or can result after processing which removes minerals and other colour-bearing compounds. The kaolinite used for the present study is natural kaolin.

Kaolinite is formed by weathering or hydrothermal alteration of alumino-silicate minerals. Granitic rocks are a common source of kaolinite, because they are rich in feldspar. Kaolinite, because it does not absorb water, does not expand when it comes in contact with water.

Kaolinite consists of SiO_2 (~55%) and Al_2O_3 (~45%) with a particle size on the order of ~ 2–10 microns. The pH is ~5.5–7.

4. Electrical features of kaolinite under pressure

The kaolinite specimen studied here has a diameter of C_s and a thickness of $4mm$. Different pressure measurements were done at $(0 - 4.5Kb)$ at a frequency of $0 - 4.5Kb$ and at ($\approx 50\%$) atmospheric relative humidity. The pressures applied are uniaxial loads upon the specimen in a confining cell ($20ton \approx 1Kbar \approx 10^3 bar$, and $1bar = 10^5 N/m^2 = 10/9.8 kg/cm^2$, $1bar \approx 10^5 Pascal$).

Figures 4 and 5 show the effects of uniaxial pressure on conductance and capacitance, respectively, at various frequencies. An increase of conductance is seen with an increase in pressure (Figure 4) (Gomaa and Abou El-Anwar 2015). The capacitance, however, shows no dependence on pressure at relatively high frequencies, because the capacitance at relatively high frequencies has reached its minimum values (Gomaa 2013). At comparatively low frequencies, a noticeable increase of capacitance occurs with increasing pressure, that tends to reach a constant value at relatively higher pressures.

The influences of frequency f on conductance and capacitance with different pressures are presented in Figures 6 and 7. The variation of conductance against frequency at different pressures is shown in Figure 6. With an absence of pressure, the conductance shows frequency-independent values. Such phenomena are described in the framework of percolation threshold theories (Gomaa et al. 2000). Percolation theory describes the behaviour of connected and disconnected clusters in a random system.

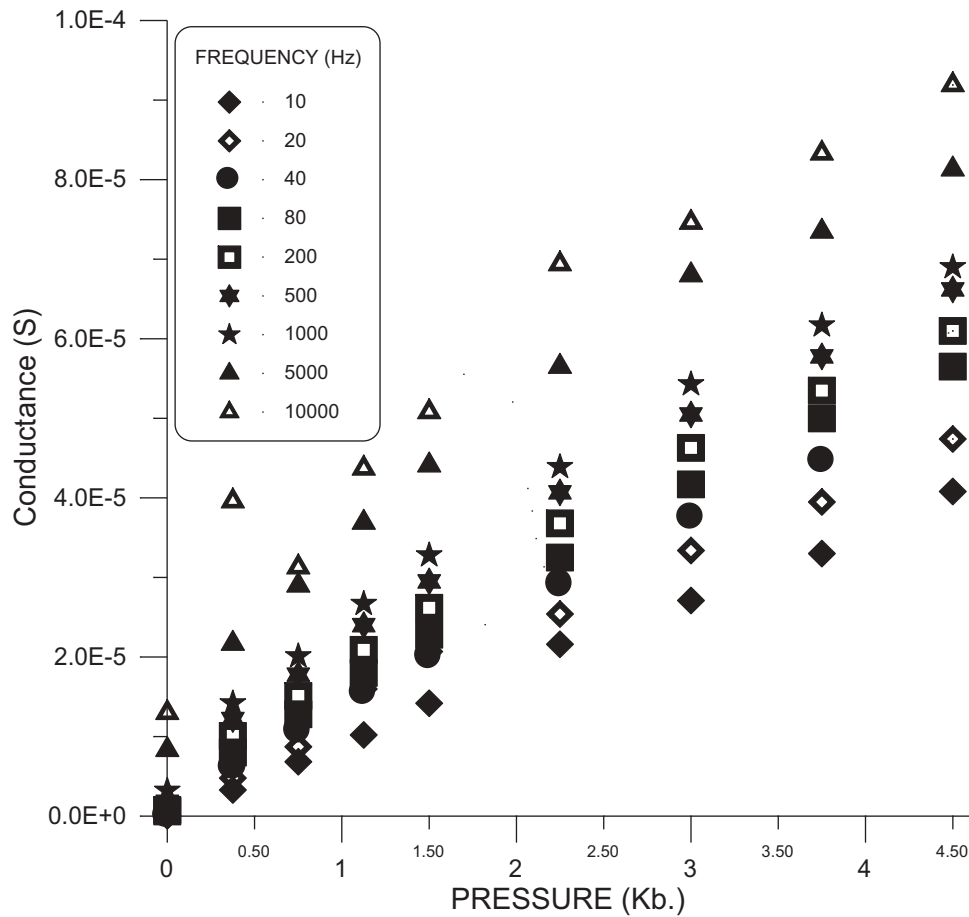Figure 7 shows the dependence of the specimen's capacitance on frequency at various pressures. At low

Figure 4. The influence of uniaxial pressure on conductance (S) at various frequencies.

pressures, a great dependence is noticed. At higher pressures, the specimen shows a lower dependence on frequency. Such behaviour can be considered, also, in the framework of percolation theory (Gomaa and Kassab 2016, 2017; Gomaa and Abou El-Anwar 2017).

The dependence of measured conductance and capacitance on applied pressure shows a great dependence (steep sloped curve) on pressure in a low-pressure range (up to nearly 1 Kb). At higher pressures a constant conductance is obtained, whereas the capacitance shows a tendency to decrease with increasing pressure. This behaviour of conductance and capacitance at higher pressures can be discussed in the framework of percolation theory. At such relatively high pressure, there is a possibility of an increase in the continuous paths of the conductor (Gomaa 2006). The dependence of conductance and capacitance on the applied frequency was found to be similar to that obtained by Olhoeft (1977). The interpretation for the samples assumed the remaining surface impedance on the kaolinite particle surface was due to remaining water (humidity), the chemical reaction and charge transport along the surface of the kaolinite particles. With increasing pressure, the pore voids between particles decrease and the conducting paths of water increase.

Figures 8–16 show data representation in the Z-plane. Figure 8 shows a kaolinite specimen measured without any external pressure and at normal atmospheric conditions of temperature ($\approx 20^0 C$) and a relative atmospheric humidity of $\approx 20^0 C$. In Figure 8, the interface impedance between grains (Z_i) is defined as ($Z_i = R_i + (1/jwc_i)$), with the capacitive part $Z_i = R_i + (1/jwc_i) \gg (R_i)$ (the real part).

For Figures 9–16, values of ReZ and ImZ are nearly the same (within a single decade), i.e. the pressure in this range has relatively little effect compared with the differences shown in Figure 8, with no pressure. As the uniaxial pressure is applied, the diffusion impedance (Warburg impedance) increases until it becomes dominant. The pressure increase may thus be postulated as equivalent to rising water content or an increase in conductor concentration (Gomaa et al. 2015a, 2015b). Increasing pressure causes a decrease in pore spaces, and accordingly increases the segment ratios of pore distances filled with water to total pore spaces after applying pressure.

The curves shown in Figures 9–16 can be separated into two parts, the low-frequency section (lower than about 400 Hz) and the relatively high frequency section (higher than about 400 Hz). The low-frequency section shows linear behaviour between the real and
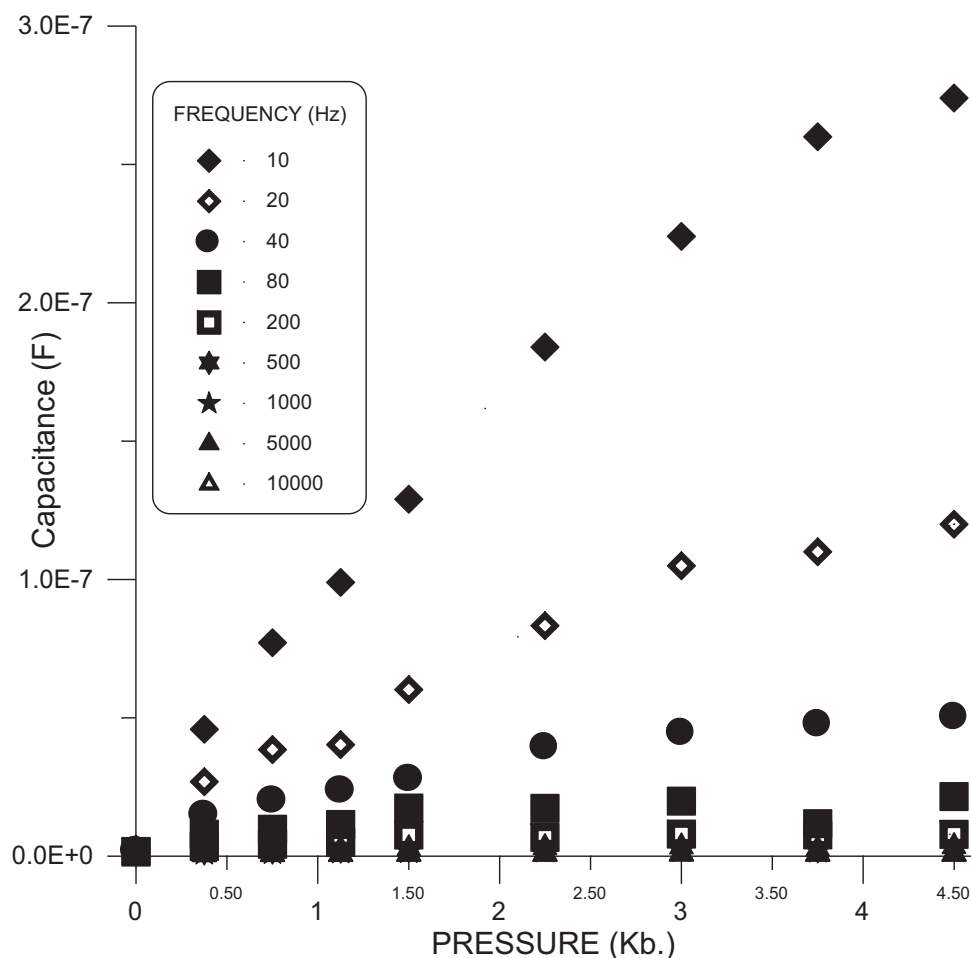
Figure 5. The influence of uniaxial pressure on capacitance (*Farad*) at various frequencies.

imaginary section of resistance. Such a straight line makes an angle of nearly 45°, with a positive orientation of *ImZ*. The relatively high frequency part can be approximated to a semicircular arc. The two regions can be postulated to be due to two distinct mechanisms whose dominant frequency ranges are far from each other. The two-region impedances are added in series (Macdonald 1974). As water content increases, or alternatively the external uniaxial pressure increases, then the contribution of each of these two mechanisms varies. The first mechanism, acting in the relatively higher frequencies, is represented by a nearly semicircular arc, whereas the one acting at the relatively lower frequencies is described by a nearly straight line of slope of 45° (Sen 1981a, 1981b, 1984). Hussain (1981) correlated this behaviour with that given for a measured heterogeneous chemical reaction (Vetter 1967, p. 348) plus a diffusion process (Warburg impedance), respectively, for the resulting charge carriers. He claimed that ion exchange on the surface of clay particles leads to the semicircular arc at the impedance plane of specimen as in the corresponding heterogeneous chemical reaction at an electrode (Vetter 1967, p. 259; Olhoeft 1976, 1980, 1985). The straight line of 45° inclination corresponds to

diffusion of the resulting charges with water content (Vetter 1967, p. 200). As pressure is applied (0.375 *Kb*), the diffusion impedance (Warburg impedance) appears and dominates, giving rise to the extremely large dielectric constant (Minaw et al. 1972; Alvarez 1973). Pressure increase may be postulated as equivalent to a rise in water content. Increasing pressure causes a decrease in pore spaces and accordingly increases the ratio of pore distances filled with water to total pore spaces after applying pressure (Wilkinson et al. 1983; Roberts and Lin 1997).

In Figures 9–16, uniaxial loads are applied to the specimen in a confining cell, and an arc can be noticed in contact with straight-line behaviour at a low frequency range. This straight line is ascribed to a diffusion effect which comes from the uniaxial applied pressure. The uniaxial pressure also controls the semicircular arc (Song et al. 1986). It is more depressed at higher pressures. Consequently, the uniaxial pressure can act via two mechanisms, the diffusion impedance (line) at a relatively low frequency range and an arc in the relatively higher frequency range.

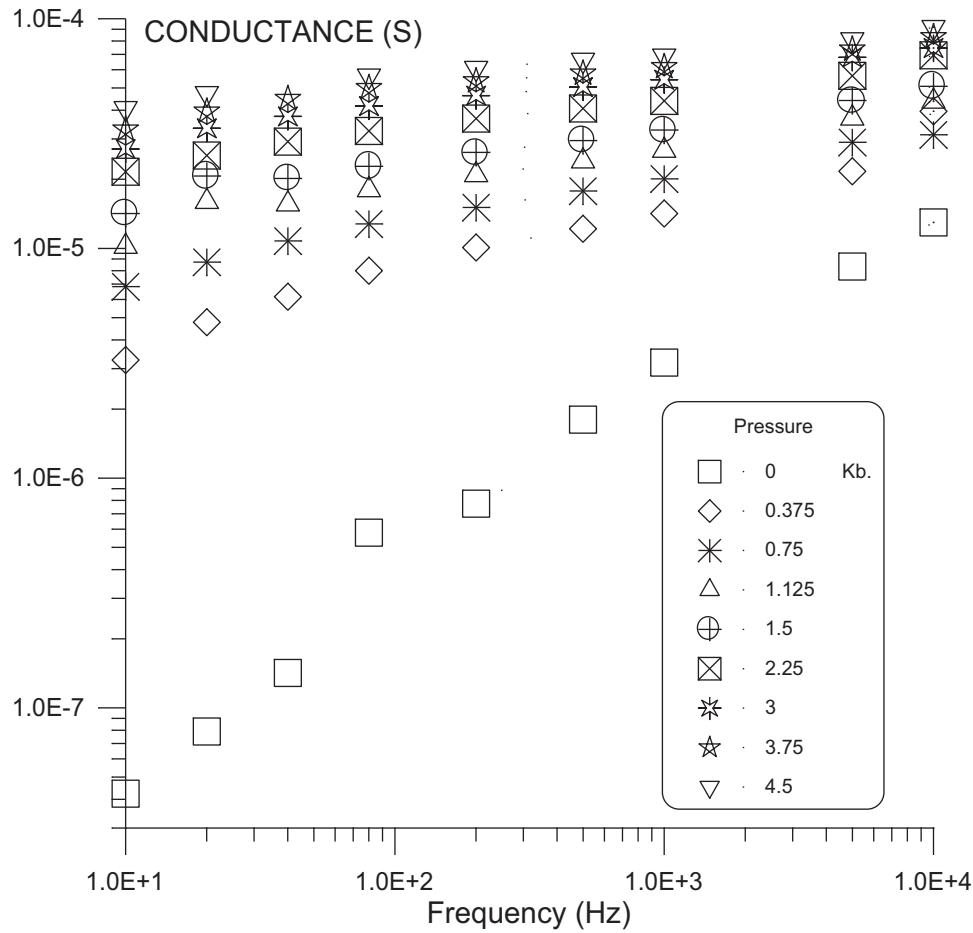The equivalent circuit of impedance is presented in Figure 17, representing the attitude of specimens

Figure 6. The influence of frequency on conductance at various pressures.

(Macdonald 1974; Kassab et al. 2017). Here, C_g and R_∞ represent the bulk features of the bulk material (arc 3 in the impedance plane Figure 15(b)), i.e. the specimen resistance and capacitance at higher frequencies (radio frequencies), where the response of water vapour (humidity) is neglected (Leroy et al. 2008). Arc 3 does not appear at the applied frequency range given here. Arc 2 represents a chemical reaction, R_∞, which occurs at frequencies relatively lower than radio frequency (lower than arc 3). Arc two can be observed in Figures 8–16. Arc 1 represents diffusion impedance or Warburg impedance Z_w (Gomaa et al. 2009, 2018). It is represented by a straight line making an angle of 45° with positive orientation of real (Z). This impedance can be seen in Figures 8–16. It occurs at frequencies relatively lower than the frequencies of arc 2 (Last and Thouless 1971; Hill and Jonscher 1983).

For experimental data, corresponding to the relatively high-frequency semicircular arc (400 Hz $<f$ < 10 KHz), for a humid kaolinite specimen under pressure, a circuit is suggested to represent the presence of a thin film of water on the surface of the humid kaolinite particles and the presence of air gaps between particles. Surface impedance on the humid kaolinite particle surfaces represents the charge transport along particle surfaces resulting from the chemical reaction due to the presence of water. The humid kaolinite particles are connected or isolated by pore spaces or by the humidity of water layers. The response to pressure is to reduce the pore voids between particles (Knight and Nur 1987; Knight and Abad 1995).

The impedance plane representation of the specimen under various pressures shows a relaxation time distribution (distribution of semicircles), which may be due to the presence of particles of different sizes and different charge mobilities (Figures 8–16).

Such charge carriers form an atmosphere of ions, which forms a diffuse double layer. The diffused double layer charge carriers are separated from the kaolinite particles by the well-known stern (solid) double layer (Grant 1958; Schurr 1964). The ions of the diffused double layer are weakly attached to the kaolinite particle surface (Gomaa et al. 2019, Khater et al. 2019a, 2019b; Melegy et al. 2019; Gomaa 2020; Gomaa and Kenawy 2020). These diffuse double layer ions can move in the water film (humidity) surrounding the particles.
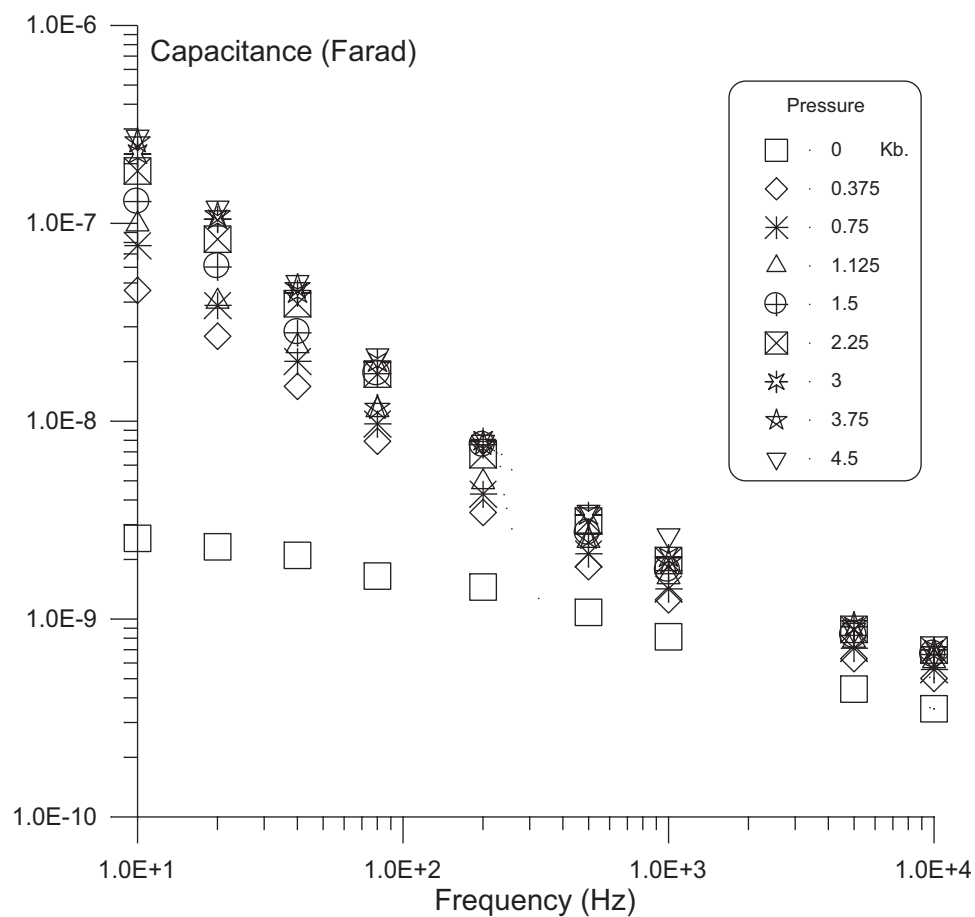
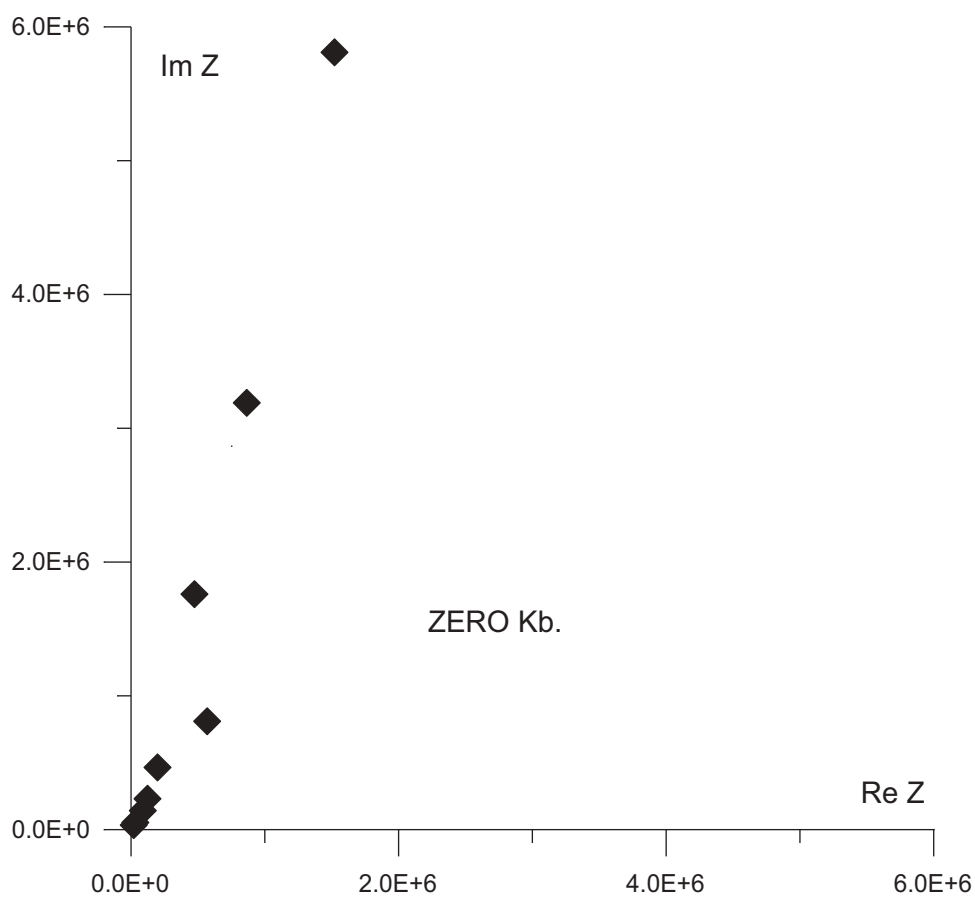**Figure 7.** The influence of frequency on capacitance at different pressures.

Figure 8. Complex impedance plane plot without any external pressure (experimental).
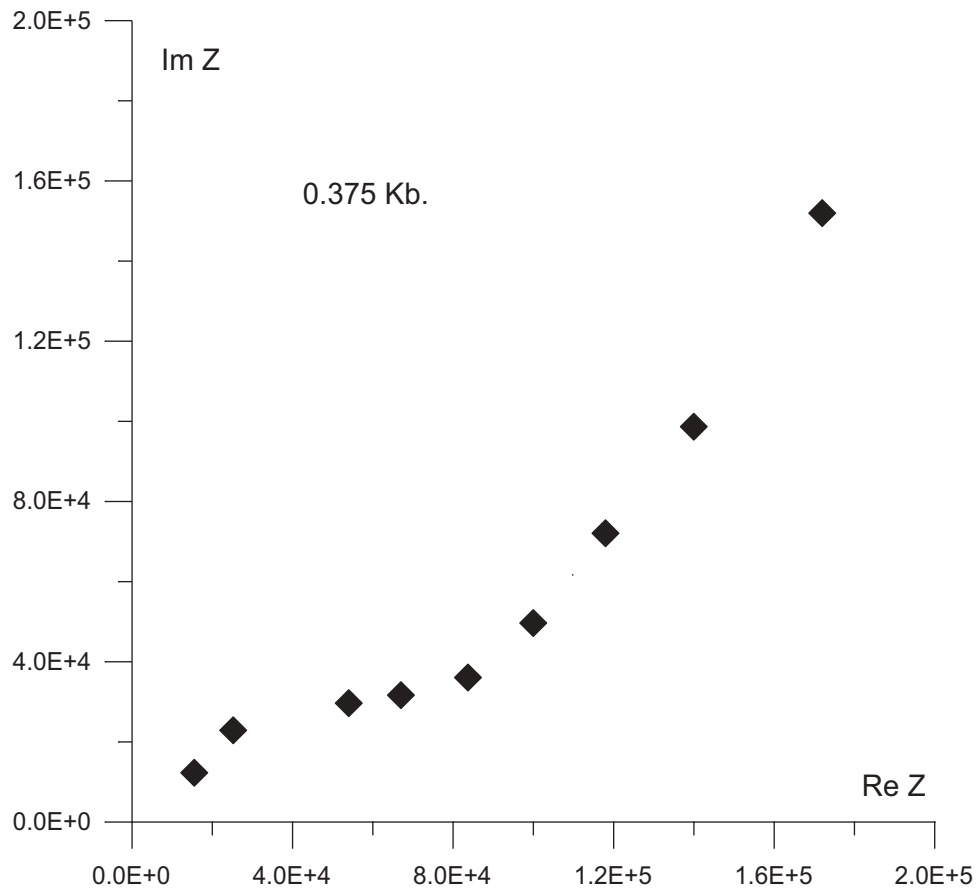
Figure 9. Experimental values of impedance (Z) for the measured kaolinite specimen with an external pressure of Z.
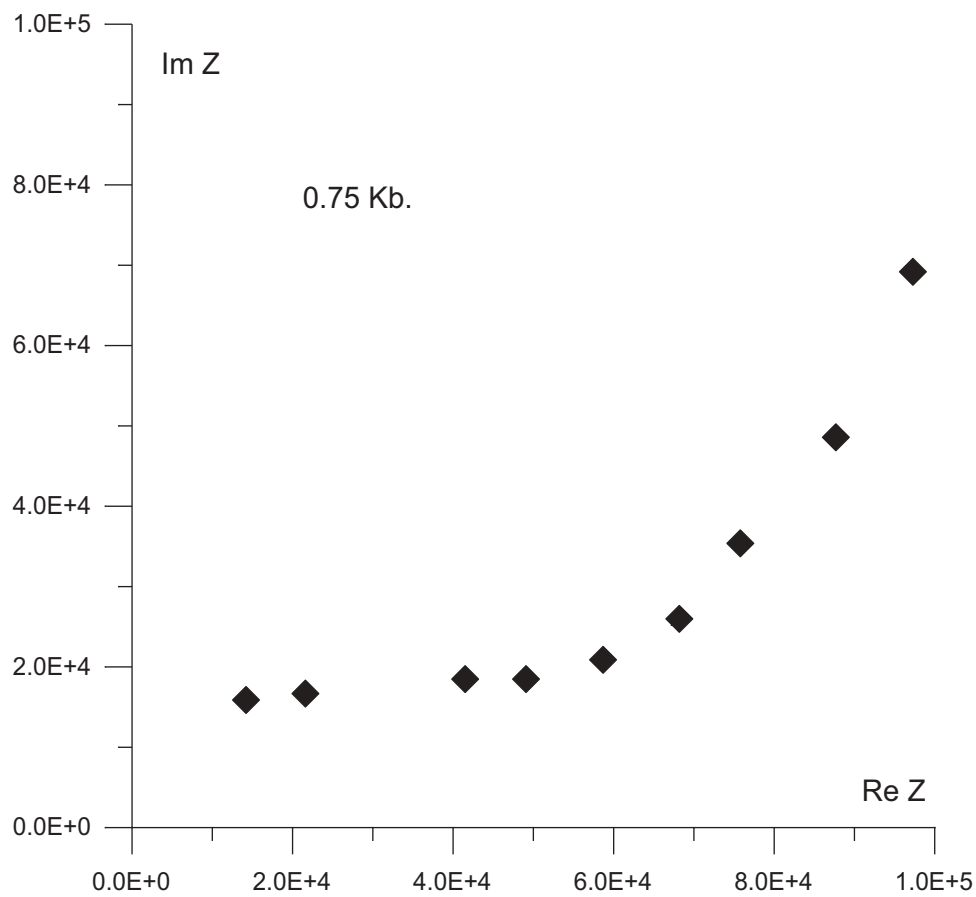

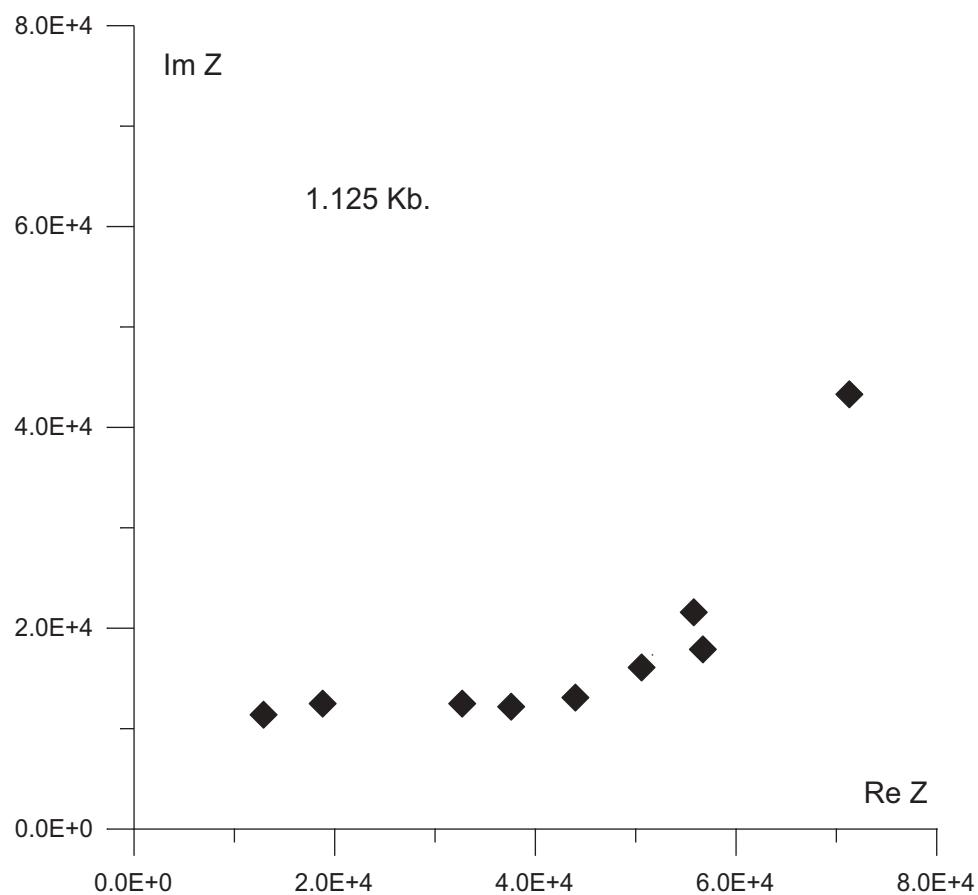**Figure 10.** Experimental values of impedance (Z) for the measured kaolinite specimen at a pressure of 0.75*Kb*.

Figure 11. Experimental values of impedance (0.75*Kb*.) for the measured kaolinite specimen at a pressure of 1.125*Kb*.
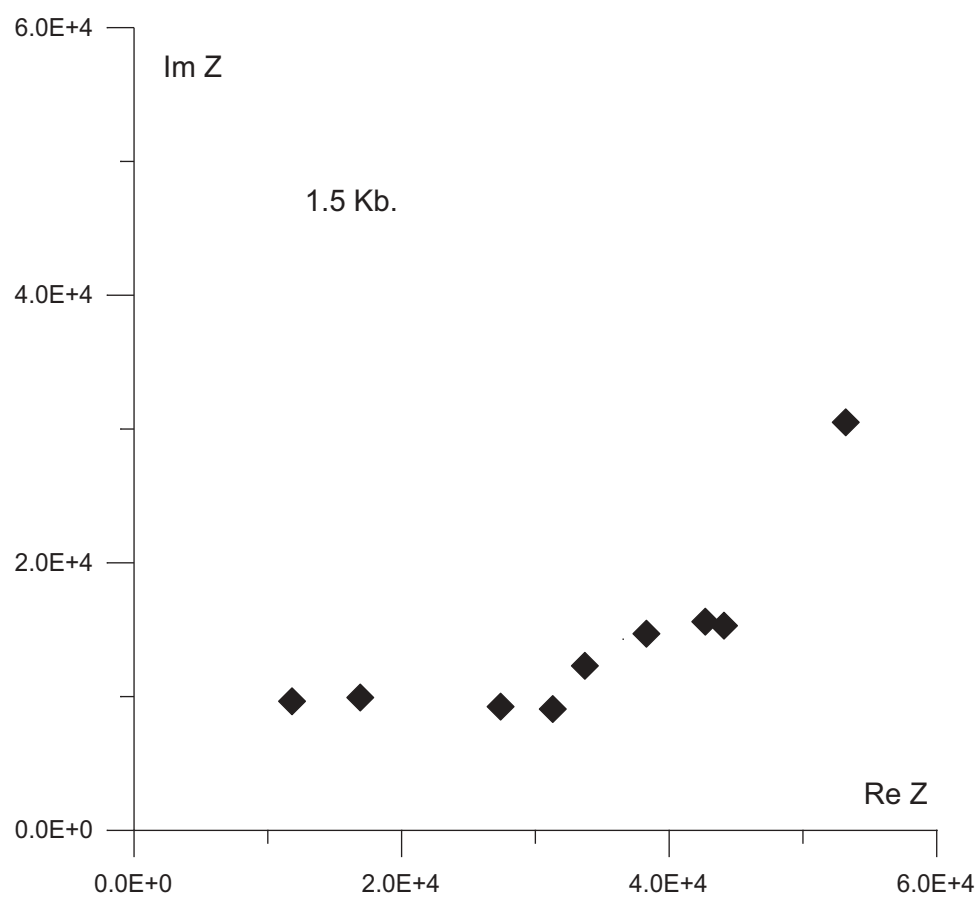

Figure 12. Experimental values of impedance (Z) for the measured kaolinite specimen at a pressure of 1.5*Kb*.
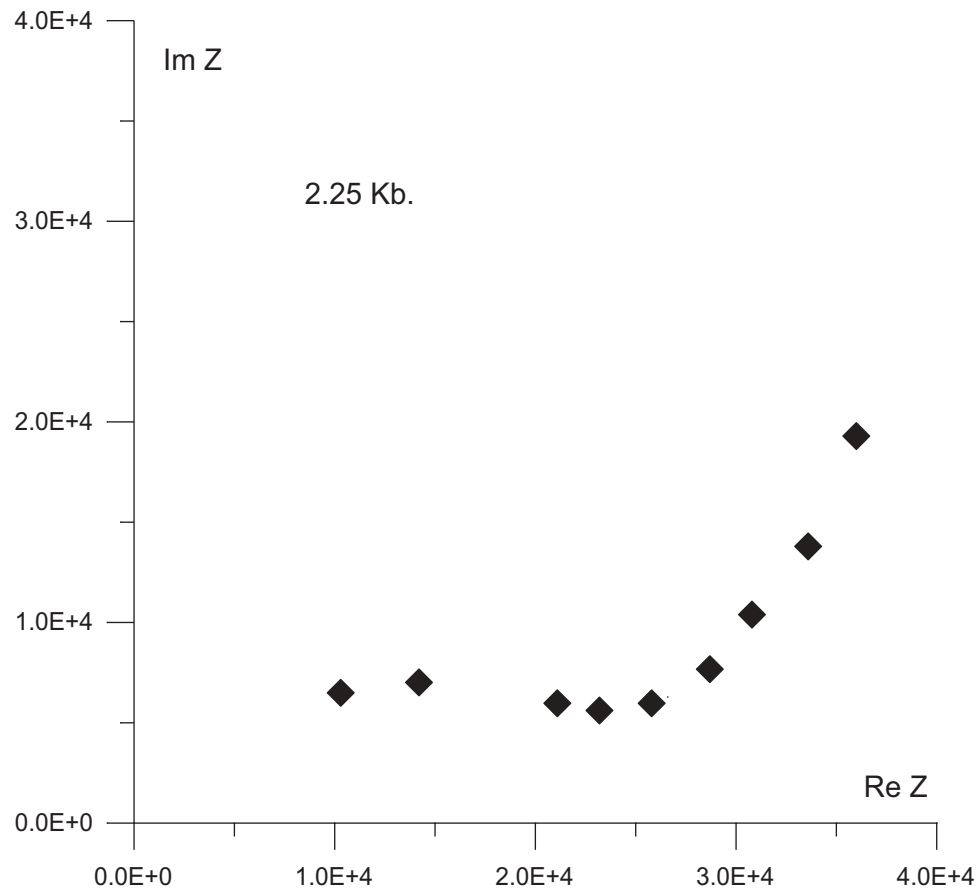
Figure 13. Experimental values of impedance (*Z*) for the measured kaolinite specimen at a pressure of *Z*.
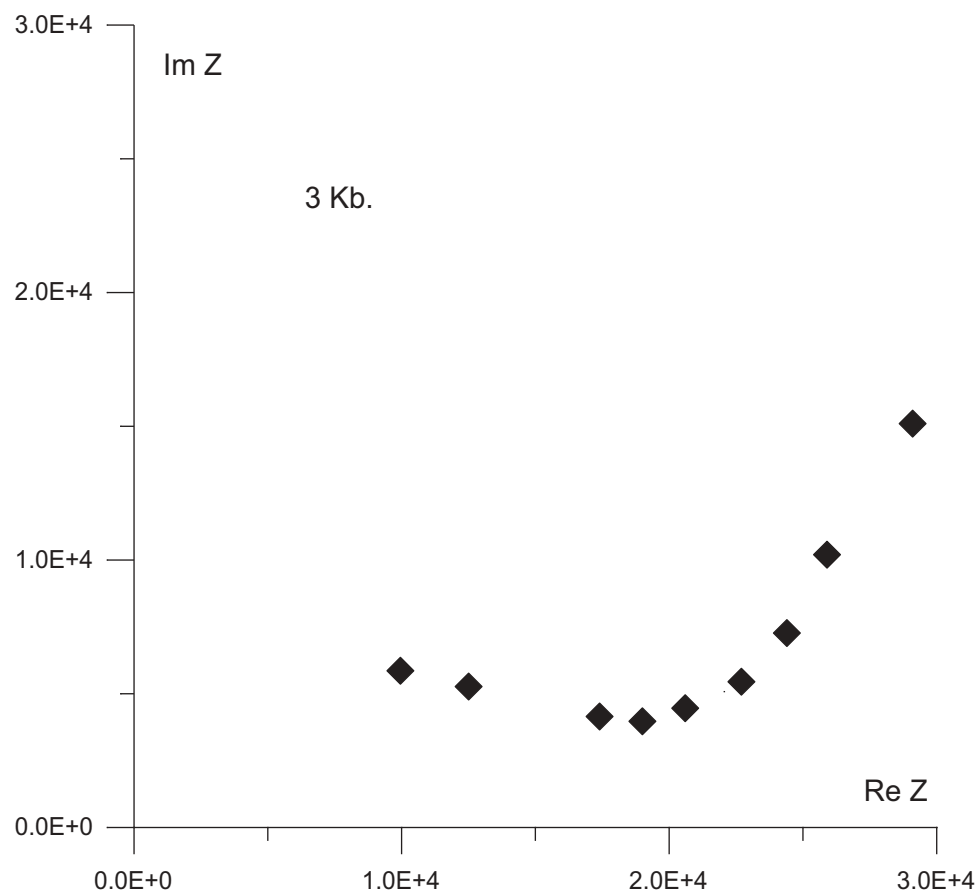

Figure 14. Experimental values of impedance (2.25*Kb*.) for the measured kaolinite specimen at a pressure of 3*Kb*.
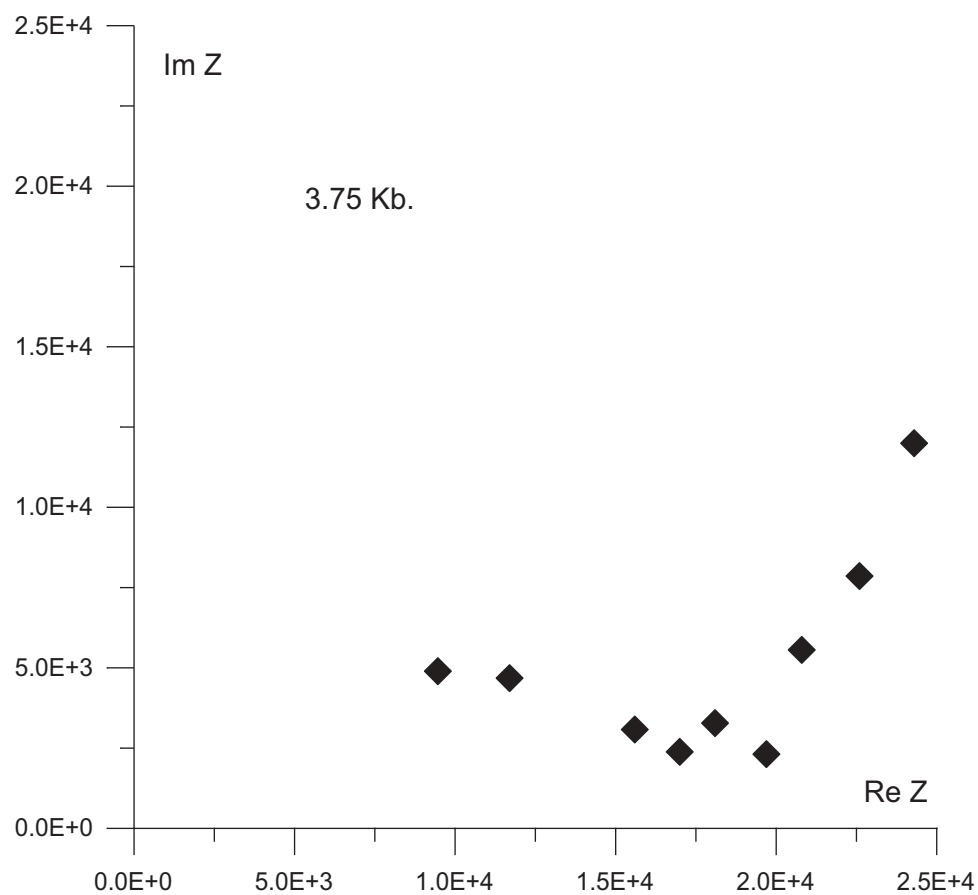
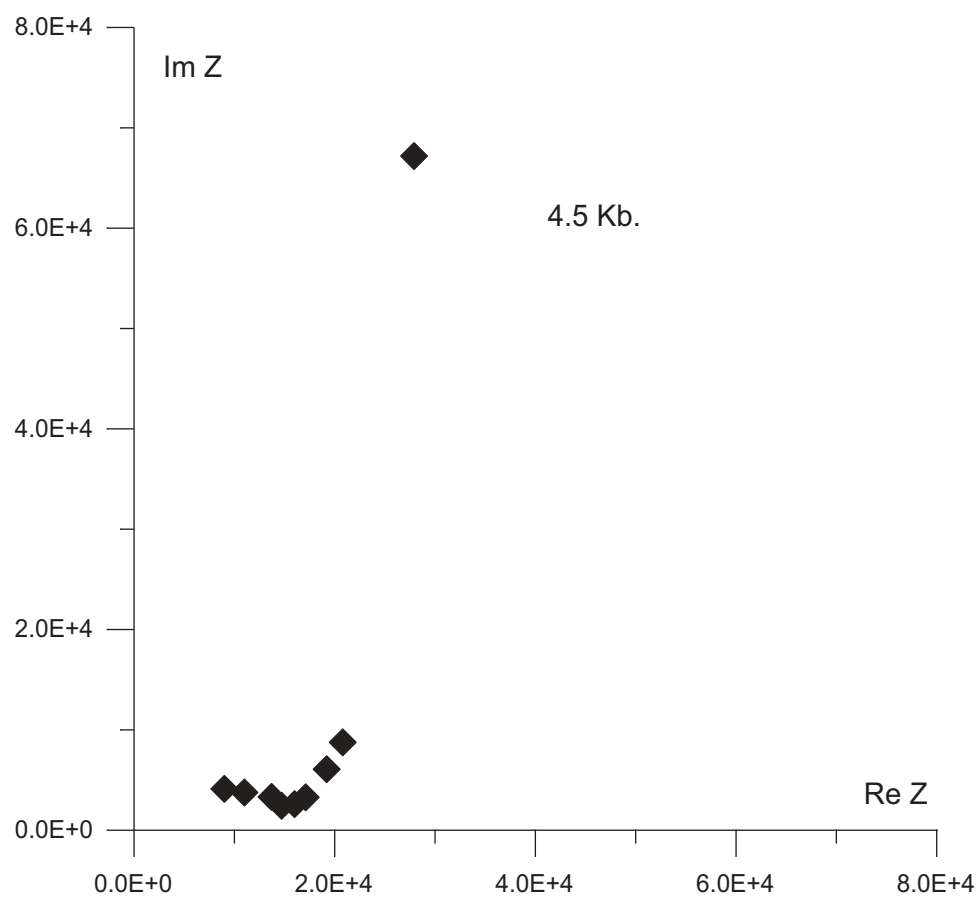**Figure 15.** Experimental values of impedance (*Z*) for the measured kaolinite specimen at a pressure of 3.75*Kb*.

Figure 16. Experimental values of impedance (*Z*) for the measured kaolinite specimen at a pressure of 4.5*Kb*.
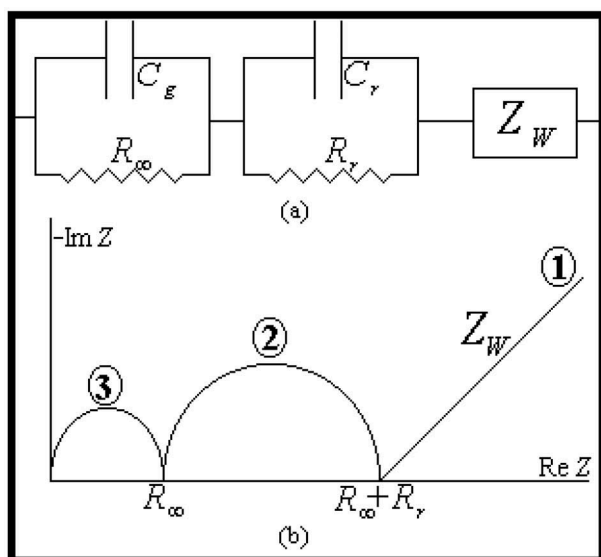
Figure 17. (a) Equivalent circuit representing the behaviour of the studied samples. (b) The impedance plane for the equivalent circuit.

5. Conclusion

Electrical features of a kaolinite sample, with relative atmospheric humidity of (Z), were measured with pressure (up to $\approx 4.5Kb$) at a frequency of $10 - 10^4$ Hz. The intention was to try to interpret experimental data for a kaolinite specimen under various pressures. Without pressure, the AC conductivity dominates in the specimen (Conductance $\propto$ f) . If external uniaxial pressure is applied, the dominance of the AC conductivity decreases while percolation threshold effects increase. The effect of specimen capacitance on the frequency at discrete pressures can also be described in the framework of percolation threshold theory. From the impedance plane representation of data, two mechanisms arise due to the application of external uniaxial pressure: the diffusion impedance mechanism and the interfacial impedance mechanism. The latter mechanism acts simultaneously with the surface chemical reaction mechanism (Debye behaviour) to give a depressed arc. This depressed arc means a relaxation of the time distribution. Further work along these lines may help in creating a model for these data.

Disclosure statement

No potential conflict of interest was reported by the author.

ORCID

Mohamed Mahmoud Gomaa http://orcid.org/0000-0002-8556-4555

References

Abou El-Anwar E, Gomaa MM. 2013. Electrical properties and geochemistry of carbonate rocks from the Qasr El-Sagha formation, El-Faiyum, Egypt. Geophys Prospect. 61:630–644.

Abou El-Anwar E, Gomaa MM. 2016. Electrical, mineralogical, geochemical and provenance of Cretaceous black shales, Red Sea Coast, Egypt. Egypt J Pet. 25:323–332.

Alvarez R. 1973. Complex dielectric permittivity in rocks: a method for its measurement and analysis. Geophys. 38 (5):920–940.

Arulanandan K. 1969. Hydraulic and electrical flows in clays. Clays Clay Miner. 17:63–76.

Bockris J, Gileady E, Muller K. 1966. Dielectric relaxation in the electric double layer. J Chem Phys. 44:1445–1456.

Borner F, Gruhne M, Schon J. 1993. Contamination indications derived from electrical properties in the low frequency range. Geophys Prosp. 41:83–98.

Brace WF, Orange AS, Madden TR. 1965. The effect of pressure on the electrical resistivity of water- saturated crystalline rocks. J Geophys Res. 70(22):5669–5678.

Chew WC, Sen PN. 1982. Dielectric enhancement due to electro-chemical double layer: thin double layer approximation. J Chem Phys. 77(9):4683–4693.

Cosenza P, Ghorbani A, Revil A, Zamora M, Schmutz M, Jougnot D, Florsch N. 2008. A physical model of the low-frequency electrical polarization of clay-rocks. J Geophys Res. 113:B08204. doi:10.1029/2007JB005539

Garrouch AA, Sharma MM. 1994. The influence of clay content, salinity, stress and wettability on the dielectric properties of brine- saturated rocks: 10 Hz to 10 MHz. Geophysics. 59(6):909–917.

Gomaa MM. 2006. Interpretation of electrical properties for humid and saturated hematitic sandstone sample. Presented at the 68th Conference and Exhibition incorporating SPE Europe: European Association of Geoscientists and Engineers (EAGE), Oral H021, Session "Gravity, Magnetics, Mining and Geothermal", Opportunities in Mature Areas 4; June 12–15; Vienna, Austria. p. 2182–2186.

Gomaa MM. 2008. Relation between electric properties and water saturation for hematitic sandstone with frequency. Ann Geophys. 51(5/6):801–811.

Gomaa MM. 2009. Saturation effect on electrical properties of hematitic sandstone in the audio frequency range using non-polarizing electrodes. Geophys Prospect. 57:1091–1100.

Gomaa MM. 2013. Forward and inverse modeling of the electrical properties of magnetite intruded by magma, Egypt. Geophys J Int. 194(3):1527–1540.

Gomaa MM. 2020. Homogeneous mixture of hematite and its electrical properties. Mater Chem Phys. 243:122584. in press. doi:10.1016/j.matchemphys.2019.122584

Gomaa MM, Abou El-Anwar E. 2015. Electrical and geochemical properties of tufa deposits as related to mineral composition in South Western Desert, Egypt. J Geophys Eng. 12(3):292–302.

Gomaa MM, Abou El-Anwar E. 2017. Electrical, mineralogical, and geochemical properties of Um Gheig and Um Bogma Formations, Egypt. Carbonates Evaporites. 34:1251–1264.

Gomaa MM, Alikaj P. 2009. Effect of electrode contact impedance on a. c. electrical properties of wet hematite sample. Mar Geophysl Res. 30(4):265–276.

Gomaa MM, Elnasharty M, Rizo E. 2019. Electrical properties speculation of contamination by water and gasoline on sand and clay composite. Arabian J Geosci. 12. in press. doi:10.1007/s12517-019-4767-4

Gomaa MM, Elsayed RM. 2006. Thermal effect of magma intrusion on electrical properties of magnetic rocks from hamamat sediments, NE Desert, Egypt. Presented at the

68th Conference and Exhibition incorporating SPE Europe: European Association of Geoscientists and Engineers (EAGE), Poster P328, Session " Gravity, Magnetics, Mining and Geothermal ", Opportunities in Mature Areas 6; June 12–15; Vienna, Austria. p. 3550–3555

Gomaa MM, Elsayed RM. 2009. Thermal effect of Magma intrusion on electrical properties of magnetic rocks from hamamat sediments, NE Desert, Egypt. Geophys Prospect. 57(1):141–149.

Gomaa MM, Hussain SA, El- Diwany EA, Bayoumi AE, Ghobashy MM. 2000. Modeling of A. C. electrical properties of humid sand and the effect of water content. Society of Exploration Geophysicists (SEG), International Exposition and 70th Annual Meeting. Vol. 19 (1); Calgary, Alberta, Canada. p. 1850–1853.

Gomaa MM, Kassab M. 2016. Pseudo random renormalization group forward and inverse modeling of the electrical properties of some carbonate rocks. J Appl Geophys. 135:144–154.

Gomaa MM, Kassab M. 2017. Forward and inverse modelling of electrical properties of some sandstone rocks using renormalisation group method. Near Surf Geophys. 15 (5):487–498.

Gomaa MM, Kassab M, El-Sayed NA. 2015a. Study of petrographical and electrical properties of some Jurassic carbonate rocks, north Sinai, Egypt. Egypt J Pet. 24 (3):343- 352.

Gomaa MM, Kassab M, El-Sayed NA. 2015b. Study of electrical properties and petrography for carbonate rocks in the Jurassic Formations: Sinai Peninsula, Egypt. Arabian J Geosci. 8(7):4627–4639.

Gomaa MM, Kenawy SH. 2020. Electrical and physical properties of ceramic whiskers from Al2O3 -CaB6 system. Expert Fachmedien GmbH: Interceram. in press.

Gomaa MM, Metwally H, Melegy A. 2018. Effect of concentration of salts on electrical properties of sediments, Lake Quaroun, Fayium, Egypt. Carbonates Evaporites. 34 (3):721-729.

Gomaa MM, Shaltout A, Boshta M. 2009. Electrical properties and mineralogical investigation of Egyptian iron ore deposits. Mater Chem Phys. 114(1):313–318.

Grant FA. 1958. Use of complex conductivity in the representation of dielectric phenomena. J Appl Phys. 29(1):76–79.

Hill RM, Jonscher AK. 1983. The dielectric behavior of condensed matter and its many- body interpretation. Contemp Phys. 24(1):75–110.

Hussain SA. 1981. ElektrischeEigenschaften von HamatitischenErzen und Kaolinit und ihreAbhangigkeit von einigenausserenBedingungen [Doctor der Naturwissencaften]. Akademie der Wissenschaften der DDR.

Hussain SA. 1997. Pressure effect on electrical properties of kaolinite clay mineral. Egypt J Phys. 28(1–2):1–16.

Jonscher AK. 1973. Carrier and matrix losses in solid dielectrics. 1972 Annual report conference on Electrical insulation and dielectric phenomena; Washington D. C.: Natn: Academy of Sci. p. 418–425.

Jonscher AK. 1975. The interpretation of non- dielectric admittance and impedance diagrams. Phys Stat Sol(a). 32:665–675.

Jonscher AK. 1977. Review article the universal dielectric response. Nature. 267:673–679.

Jonscher AK. 1999a. Dielectric relaxation in solids. J Phys D: Appl Physics. 32:R57- R70.

Jonscher AK. 1999b. Review article dielectric relaxation in solids. J Phys D: Appl Phys. 32:R57- R70.

Jougnot D, Revil A, Leroy P. 2009. Diffusion of ionic tracers in the Callovo-Oxfordian clay-rock using the Donnan equilibrium model and the electrical formation factor. Geochim Cosmochim Acta. 73(10):2712–2726. doi:10.1016/j.gca.2009.01.035

Kassab M, Gomaa MM, Lala A. 2017. Relationships between electrical properties and petrography of El-Maghara sandstone formations, Egypt. NRIAG J Astron Geophys. 6:162-173.

Khater GA, Gomaa MM, Junfeng Kang, YunlongYue M, Mahmoud A. 2019a. Thermal, electrical and physical properties of glasses based on basaltic rocks. Silicon. 4. 12 (3):645–653

Khater GA, Gomaa MM, Kang J, Mahmoud MA. 2019b. EffectofCaO/SiO2 molarratioontheelectricalandphysical-propertiesofbasalticglassmaterials. Heliyon. 4. 5(2). https://doi.org/10.1016/j.heliyon.2019.e01248.

Klein JD, Sill WR. 1982. Electrical properties of artificial clay- bearing sandstone. Geophys. 47(11):1593–1605.

Knight RJ, Abad A. 1995. Rock/water interaction in dielectric properties: experiments with hydrophobic sandstones. Geophys. 60(2):431–436.

Knight RJ, Nur A. 1987. The dielectric constant of sandstones, 60 kHz to 4 MHz. Geophys. 52:644–654.

Last BJ, Thouless DJ. 1971. Percolation theory and electrical conductivity. Phys Rev Lett. 27(25):1719–1721.

Leroy P, Revil A. 2004. A triple-layer model of the surface electrochemical properties of clay minerals. J Colloid Interface Sci. 270(2):371–380. doi:10.1016/j.jcis.2003.08.007

Leroy P, Revil A. 2009. A mechanistic model for the spectral induced polarization of clay materials. J Geophys Res. 114:B10202.

Leroy P, Revil A, Kemna A, Cosenza P, Ghorbani A. 2008. Complex conductivity of water-saturated packs of glass beads. J Colloid Interface Sci. 321(1):103–117.

Levitskaya TM. 1984. Dielectrical relaxation in rock, Izvestiya. Earth Phys. 20(10):777–780.

Levitskaya TM, Sternberg BK. 1996a. Polarization processes in rocks 1. Complex dielectric permittivity method. Radio Sci. 31(4):755–779.

Levitskaya TM, Sternberg BK. 1996b. Polarization processes in rocks 2. Complex dielectric permittivity method. Radio Sci. 31(4):781–802.

Lockhart NC. 1980. Electrical properties and the surface characteristics and structure of clays. II. Kaolinite—A nonswelling clay. J Colloid Interface Sci. 74(2):520–529. doi:10.1016/0021-9797(80)90221-0

Macdonald J. R., 1974. Some AC response results for solids with recombining space charge, J. Phys. C: Solid State Phys. 7:L327–L331.

Macdonald J. R. 1980. Interface effects of the electrical response of non- metallic conducting solids and liquids. IEEE Trans Elec.Insul. EI- 15(2):55–82.

Melegy A, Gomaa MM, Metwaly H, Hassan S. 2019. Geochemical and electrical properties of some heavy metals in El-Tabbin area, Egypt. Curr Sci Int. 8(1):101–108.

Minaw F, Hanna B, Mikhail FN. 1972. Relation between the dielectric constant and the dielectric loss for some Egyptian rocks. Egypt J Geol. 16(2):293–301.

Olhoeft GR. 1976. electrical properties of rocks. In: Sterns RGJ, editor. The physics and chemistry of minerals and rocks. NY: Wiley; p. 261–278.

Olhoeft GR. 1977. Electrical properties of natural clay permafrost. Can J Earth Sci. 14:16–24.

Olhoeft GR. 1980. Electrical properties of rocks. In: Touloukian YS, Judd WR, Roy RF, editors. Physical

properties of rocks and minerals. McGrow- Hill Book Co.; p. 257–330.

Olhoeft GR. 1985. low- frequency electrical properties. Geophys. 50(12):2492–2503.

Roberts J, Lin W. 1997. Electrical properties of partially saturated topopah spring tuff: water distribution as a function of saturation. Water Resour Res. 33:577–587.

Ruffet C, Gueguen Y, Darot M. 1991. Complex conductivity measurements and fractal nature of porosity. Geophys. 56 (6):758–768.

Schurr JM. 1964. On the theory of the dielectric dispersion of spherical colloidal particles in electrolyte solution. J Chem Phys. 68:2407–2413.

Schwarz G. 1962. A theory of the low frequency dielectric dispersion of colloidal particles in electrolyte solution. J Chem Phys. 66:2636–2642.

Sen PN. 1981a. Dielectric anomaly in inhomogeneous materials with application to sedimentary rocks. Appl Phys Lett. 39(8):667–668.

Sen PN. 1981b. Relation of certain geometrical features to the dielectric anomaly of rocks. Geophys. 46(12):1714–1720.

Sen PN. 1984. Short note: grain shape effects on dielectric and electrical properties of rocks. Geophys. 49(5):586–587.

Shaltout AA, Gomaa MM, Wahbe M. 2012. Utilization of standardlessanalysis algorithms using WDXRF and XRD for Egyptian Iron Ores identification. X-Ray Spectrum. 41:355–362.

Song Y, Noh TW, Lee S, Gaines R. 1986. Experimental study of the three- dimensional A. C. conductivity and dielectric constant of a conductor- insulator composite near the percolation threshold. Phys Rev B. 33 (2):904–908.

Vetter K. J. 1967. Electrochemical kinetics. In: Bruckenstein S, Howard. B, editors. Theoretical and Experimental Aspects. New York: Academic Press.

Wilkinson D, Langer JS, Sen PN. 1983. Enhancement of the dielectric constant near a percolation threshold. Phys Rev B. 28(2):1081–1087.